

# A Finite-Volume Method in General Curvilinear Coordinates for Simulation of Blood Flow Past a Stenosed Artery

**S. Pasha Zanous\* & R. Shafaghat**

Department of Mechanical Engineering,  
Babol Noshiravani University of Technology, Iran  
Email: S.pasha@stu.nit.ac.ir, rshafaghat@nit.ac.ir

\*Corresponding author

**Q. Esmaili**

Department of Mechanical Engineering,  
Ayatollah Amoli branch, Islamic Azad University, Iran  
E-mail: Qesmaili@iauamol.ac.ir

**Received: 9 December 2013, Revised: 30 June 2014, Accepted: 5 July 2014**

**Abstract:** In this study, the flow characteristics through symmetric stenosis artery are investigated. The shape of eccentricity for stenotic flows is limited by circular-cross sections and plaques usually assumed to be oriented concentrically. The governing equations are the usual Navier-Stokes equations and are numerically solved by using finite volume method in arbitrary orthogonal curvilinear coordinates. In addition, three-dimensional (3D) elliptic grid is presented, which the generating system is based on the solution of a partial differential system. To prevent serious distortion or overlapping of mesh lines, grid regularity is verified by some controlling parameter like Skewness value and maximum grid aspect ratio (MAR). The main objective of the present study is to investigate different degrees of the stenosis (45%, 55%, 65%, and 75% by area reduction) and finding the critical one playing a significant role in the development of forming sediment in the vessel wall. It is shown that the magnitude of inlet Reynolds number has strong relationship with the velocity, pressure, and wall shear stress (WSS) distributions as expected. The most important conclusion obtained from this model is the high WSS, pressure drop, and formation of large recirculation regions found in the downstream of the stenosis, especially in the case of severe stenosis that could create various pathological diseases.

**Keywords:** CFD, Normal Stenosis, Orthogonal Curvilinear Coordinates, Wall Shear Stress

**References:** Pasha Zanous, S., Shafaghat, R., and Esmaili, Q., "A Finite-Volume Method in General Curvilinear Coordinates for Simulation of Blood Flow past a Stenosed Artery", Int J of Advanced Design and Manufacturing Technology, Vol. 7/ No. 3, 2014, pp. 27-36.

**Biographical notes:** **S. Pasha Zanous** is currently MSc student of Babol Noshirvani University. His current research interest includes CFD and biomechanics. **R. Shafaghat** received his PhD in Mechanical Engineering from University of IUST, Iran 2009 and BSc in Fluid Mechanics from Sharif U.T., Iran 1997. He is currently Assistant Professor at the Department of Mechanical Engineering, Babol Noshirvani University. His current research interest includes CFD, Fuel Cell, and Internal Combustion Engine. **Q. Esmaili** is Associate Professor of Mechanical engineering at the University of Ayatollah Amoli branch, Iran. He received his PhD in Mechanical engineering from Noshirvani University, Iran. His current research focuses on CFD, thermodynamics and heat transfer.

---

## 1 INTRODUCTION

---

Atherosclerosis refers to the development of fatty deposits on the walls of the medium and large blood vessels. These fatty deposits are commonly known as atheroma or atherosclerotic plaques obstructing the normal flow of blood through the blood vessels. Atherosclerosis is the most common type of arteriosclerosis (thickening of blood vessels that carry oxygenated blood in the body) and is sometimes used as a synonym of arteriosclerosis. The blood vessels of the heart, brain, kidneys, legs and other vital organs may be affected either directly or indirectly. This is the most common cause of heart disorders and the associated cases of death in the developed countries.

In relation to the development of experimental models for flow in diseased human carotid arteries, extensive studies have been performed on flow visualization in the vicinity of stenosis under steady-state and pulsatile-flow conditions by Giddens et al., [1-3]. Stenotic artery with an unrealistic range of Reynolds number up to 15000 was studied extensively by Deshpande and Giddens [1]. In ref., flow visualization at constriction was investigated, using axisymmetric model geometries with 25%, 50% and 75% area reductions [2]. Generally, some flow parameters such as, WSS and pressure drop require accurate measurements about the artery wall experimentally, which is difficult, even for the technology presently available. Therefore, computational fluid dynamics (CFD) can play a significant role in producing relatively accurate data across mildly stenosed vessels.

Hence, understanding of stenotic flow has also proceeded from both analytical and computational efforts; steady flow through an axisymmetric stenosis was studied extensively by Smith using an analytical approach [4]. It has been found that the flow patterns depend strongly on the geometry of the stenosis and the upstream Reynolds number. Numerical simulation of steady flow through an axisymmetric stenosis was carried out by Deshpande et al., using a finite difference technique [5]. The obtained flow patterns were in good agreement with the experimental results of Young and Tsai [6]. An LES study was conducted on the planer channel with one-sided semi-circular constriction under pulsatile flow condition in the range of Reynolds number 750 to 2000, with focus on the spectral analysis of the turbulent flows [7]. They observed that magnitude of the kinetic energy and specific dissipation increased within the stenosis with increasing Reynolds numbers.

Direct numerical simulation was carried out by Varghese et al., [8], to replicate the benchmark experimental results of Ahmed and Giddens [2]. They extended their work for asymmetric stenosis with the same degree of stenosis, %75, under steady and

pulsatile flow condition [9]. They showed that acceleration of the fluid through the stenosis resulted in WSS magnitudes exceeding upstream levels more than 30 times; however low WSS levels are accompanied with the flow separation zones formed immediately downstream of the stenosis. Another study was carried out by Sousa et al., applied the finite element method to solve the stenotic flow through a 3D artery [10]. Velocity and WSS fields were visualized for a better understanding of flow characteristics such as distributions of the flow pattern, stagnation flow, and recirculation zones in their study.

The effect of stenosis shape on blood flow through an artery is visualized by Singh and Shah [11]. The blood is modelled as power-law fluid in a uniform circular tube with an axially non-symmetric but radially symmetric stenosis. It has been found that the resistance to flow, wall shear stress, and apparent viscosity decrease as stenosis shape parameter increase but they increase as stenosis size and stenosis length increase. Recently, a computational simulation in a carotid stenotic artery with varying pulsatile inlet profile has been conducted by Senol and Serdar, which 3D transient NS equations was solved in actual domain, using the proposed boundary conditions [12]. In addition, effects of different input conditions on the results were discussed. The most important conclusion obtained from their model is the existence of negative relation between velocity at several inner points of the internal carotid artery and velocity at the inlet of the common carotid artery.

In this paper, a considerable effort is devoted to implementing 3D finite volume method (FVM) in generalized body fitted coordinate in non-rectangular domain. Then, it can be concluded that the geometric limitation is removed by adopting this coordinate system in the in-house code. Thus, this paper provides insight into the numerical simulation of stenosis artery by applying the exact geometry of stenosis model without attending to the complicate procedure for complex geometry in Cartesian coordinate. Furthermore, our aim is to investigate the effect of different degrees of stenosis on the flow characteristics and illustrate the critical one, which causes serious damage to the vessel wall. It is noted that the possibility of the endothelium destruction is higher in the regions where wall shear stresses are beyond the range of 1-42  $\text{n/m}^2$  that is the safe bandwidth of WSS [13].

---

## 2 NUMERICAL PROSEDURE

---

### 2.1. Physical model

Simple models of symmetric artery with different degrees of circular stenosis considered in the present

study are shown in Fig. 1. The diameter of the arteries D is 25.4 mm and the domains extending to 4D and 17D upstream ( $L_u$ ) and downstream ( $L_d$ ) of the stenosis, respectively. The length of stenosis ( $L_s$ ) is 1.5D in all models, as well.

The stenosis severity is calculated using [8]:

$$S = (1 - A_1 / A_2) \times 100 \quad (1)$$

Where  $A_1$  and  $A_2$  are the cross-sectional areas at the throat and inlet of all models, respectively.

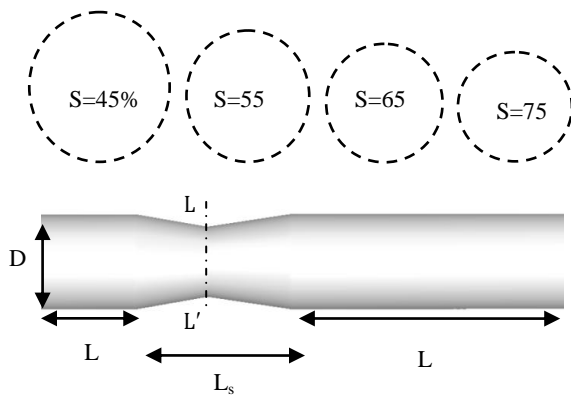


Fig. 1 Schematic of a symmetric stenosis with 45%, 55%, 65%, and 75% area reduction

### 2.2. Grid generation

Traditional methods of simulating arbitrary shape geometries were mostly performed in Cartesian coordinates, which cause some errors related to the grid precision.

Finer grid may lead to more computation cost. In this study, the general curvilinear coordinates is adopted, it helps transform the physical domain into a simple domain in the transformed space. In order to obtain a grid in the transformed space, a grid system generating method needs to be developed. The simplest equation that could be used to generate the grid is the Laplace's equations [14]:

$$\nabla^2 \xi_i = 0, \quad i = 1, 2, 3 \quad (2)$$

The above partial differential equations are subject to a set of Dirichlet boundary conditions. First, the boundaries of the domain are identified and initial mesh is obtained by using an algebraic method (here, TFI [15]). Then, Eq. (2) is transformed into the computational domain where the Cartesian coordinates are the dependent variables [15]:

$$\begin{aligned} \alpha_{11} X_{\xi\xi} + \alpha_{22} X_{\eta\eta} + \alpha_{33} X_{\zeta\zeta} + 2\{\alpha_{12} X_{\xi\eta} + \alpha_{13} X_{\xi\zeta} + \alpha_{23} X_{\eta\zeta}\} &= 0 \\ \alpha_{11} Y_{\xi\xi} + \alpha_{22} Y_{\eta\eta} + \alpha_{33} Y_{\zeta\zeta} + 2\{\alpha_{12} Y_{\xi\eta} + \alpha_{13} Y_{\xi\zeta} + \alpha_{23} Y_{\eta\zeta}\} &= 0 \\ \alpha_{11} Z_{\xi\xi} + \alpha_{22} Z_{\eta\eta} + \alpha_{33} Z_{\zeta\zeta} + 2\{\alpha_{12} Z_{\xi\eta} + \alpha_{13} Z_{\xi\zeta} + \alpha_{23} Z_{\eta\zeta}\} &= 0 \end{aligned} \quad (3)$$

The coefficients of equations (3) are obtained in [15]. Finally, the grid points are generated using equations (3) in an iterative elliptic loop where algebraic initial mesh is its initial condition.

### 2.3. Grid quality

Grid quality is important for minimizing computational error. A well-designed grid should be orthogonal. Additionally, grid aspect ratios close to one are important for good conditioning of the discrete operator, as well as for reducing errors in derivatives of the approximate solution. Therefore, for obtaining 3D, clustered, and smooth grid, grid regularity should be verified. The verification is performed by some controlling parameter like Skewness value [16] and MAR [17].

#### 2.3.1. MAR

MAR is used to study the quality of the resulting grids and preventing grid lines from collapsing on to each other. In this study, MAR is calculated from [17]:

$$\text{MAR} = \max_{i,j,k} \left( \max \left( \frac{h^{i,i+1}_{\xi jk}}{h^{j,j+1}_{\eta jk}}, \frac{h^{j,j+1}_{\eta jk}}{h^{i,i+1}_{\xi jk}}, \frac{h^{i,i+1}_{\xi jk}}{h^{k,k+1}_{\zeta jk}}, \frac{h^{k,k+1}_{\zeta jk}}{h^{i,i+1}_{\xi jk}}, \frac{h^{j,j+1}_{\eta jk}}{h^{k,k+1}_{\zeta jk}}, \frac{h^{k,k+1}_{\zeta jk}}{h^{j,j+1}_{\eta jk}} \right) \right) \quad (4)$$

Where Scale factors  $h_{\xi jk}$ ,  $h_{\eta jk}$  and  $h_{\zeta jk}$  are discretized as:

$$\begin{aligned} h^{i,i+1}_{\xi jk} &= \left[ (x_{i+1,j,k} - x_{ijk})^2 + (y_{i+1,j,k} - y_{ijk})^2 + (z_{i+1,j,k} - z_{ijk})^2 \right]^{\frac{1}{2}} \\ h^{j,j+1}_{\eta jk} &= \left[ (x_{i,j+1,k} - x_{ijk})^2 + (y_{i,j+1,k} - y_{ijk})^2 + (z_{i,j+1,k} - z_{ijk})^2 \right]^{\frac{1}{2}} \\ h^{k,k+1}_{\zeta jk} &= \left[ (x_{i,j,k+1} - x_{ijk})^2 + (y_{i,j,k+1} - y_{ijk})^2 + (z_{i,j,k+1} - z_{ijk})^2 \right]^{\frac{1}{2}} \end{aligned} \quad (5)$$

Where subscripts i, j and k represent node numbers and discretized directions.

#### 2.3.2. Skewness

At a complicated boundary, the orthogonalization will invert the grid eventually after a sufficient number of

repetitions. The verification is performed by calculating a normalized cell volume, so-called Skewness value, for each of the cells affected by the orthogonalization. The Skewness value  $\sigma$  is defined as the volume divided by the quantities  $e_1$ ,  $e_2$ , and  $e_3$ , which are the maxima of the lengths of the cell edges in the three curvilinear coordinate directions [16]:

$$\sigma = V / (e_1, e_2, e_3) \quad (6)$$

Where  $V$  is the cell volume and  $e_1$ ,  $e_2$ , and  $e_3$  are obtained in [16].

## 2.4. Governing equations

The governing equations in the computational space are (Variable  $\Phi$  is considering as a velocity components at Cartesian coordinates) [18]:

$$\begin{aligned} & \frac{1}{J} \left[ \frac{\partial}{\partial \xi} (\rho U^c) + \frac{\partial}{\partial \eta} (\rho V^c) + \frac{\partial}{\partial \zeta} (\rho W^c) \right] = 0 \\ & \frac{\partial}{\partial \xi} (\rho U^c \Phi) + \frac{\partial}{\partial \eta} (\rho V^c \Phi) + \frac{\partial}{\partial \zeta} (\rho W^c \Phi) \\ & = \frac{\partial}{\partial \xi} \left( \mu j q_{11} \frac{\partial \Phi}{\partial \xi} \right) + \frac{\partial}{\partial \eta} \left( \mu j q_{22} \frac{\partial \Phi}{\partial \eta} \right) \\ & \quad + \frac{\partial}{\partial \zeta} \left( \mu j q_{33} \frac{\partial \Phi}{\partial \zeta} \right) + JS^{CD} \end{aligned} \quad (7)$$

Where  $U^c$ ,  $V^c$ , and  $W^c$  are velocity components in computational domain:

$$\begin{aligned} U^c &= J(U\xi_x + V\xi_y + W\xi_z) \\ V^c &= J(U\eta_x + V\eta_y + W\eta_z) \\ W^c &= J(U\zeta_x + V\zeta_y + W\zeta_z) \end{aligned} \quad (8)$$

Where  $\xi$ ,  $\eta$  and  $\zeta$  are general curvilinear coordinates and determinant of inverse Jacobean is:

$$\begin{aligned} J &= x_\xi (y_\eta z_\zeta - y_\zeta z_\eta) + y_\xi (z_\eta x_\zeta - x_\eta z_\zeta) \\ & \quad + z_\xi (x_\eta y_\zeta - y_\eta z_\zeta) \end{aligned} \quad (9)$$

Source term ( $JS^{CD}$ ) is evaluated by:

$$\begin{aligned} JS &= \frac{\partial}{\partial \xi} \left[ \mu j (q_{12} \Phi_\eta + q_{13} \Phi_\zeta) \right] + \frac{\partial}{\partial \eta} \left[ \mu j (q_{12} \Phi_\xi + q_{23} \Phi_\zeta) \right] \\ & \quad + \frac{\partial}{\partial \zeta} \left[ \mu j (q_{13} \Phi_\xi + q_{23} \Phi_\eta) \right] \end{aligned} \quad (10)$$

In addition, coefficients  $q_{11}$ ,  $q_{22}$  and  $q_{33}$  are:

$$\begin{aligned} q_{11} &= \xi_x \xi_x + \xi_y \xi_y + \xi_z \xi_z \\ q_{22} &= \eta_x \eta_x + \eta_y \eta_y + \eta_z \eta_z \\ q_{33} &= \zeta_x \zeta_x + \zeta_y \zeta_y + \zeta_z \zeta_z \end{aligned} \quad (11)$$

Values  $\xi_x$ ,  $\xi_y$  and etc. are calculated from [18].

## 2.5. Boundary conditions

In the current work, the flow is assumed to be laminar, incompressible, and the wall is rigid. The blood is treated as a Newtonian fluid, which is a common assumption, used in simulating flow in large arteries [19]. Hence, Blood is modeled as a Newtonian fluid and the density is taken as constant throughout the domain in this study. Viscosity ( $\mu$ ) and density ( $\rho$ ) are taken as 0.022 kg/ms and 1600 kg/m<sup>3</sup> respectively. The inlet velocity is assumed to have a parabolic profile and convective boundary condition is applied at the outlet.

## 3 GRID INDEPENDENCY AND VALIDATION

In order to validate the applicability of the in-house code prepared in Fortran 90 in general curvilinear coordinates, 3D cylindrical tube is simulated, and numerical results are compared with analytical solution [20].

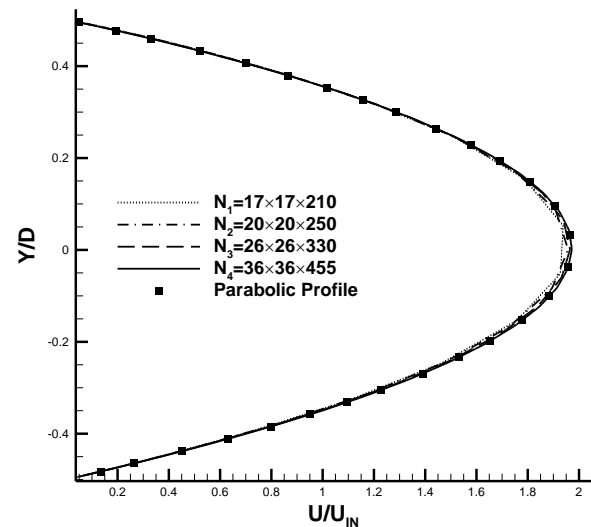
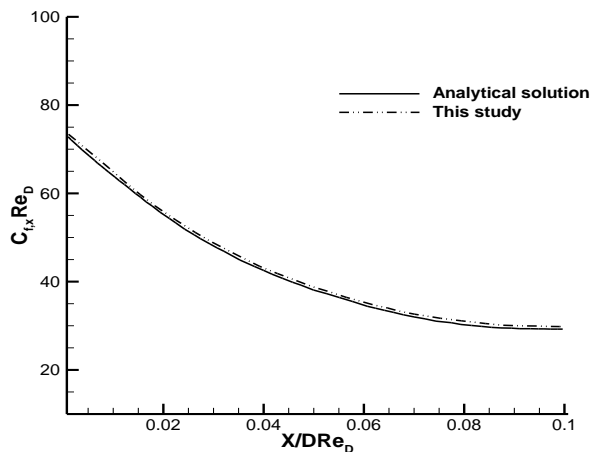


Fig. 2 Comparison of x-velocity profiles using four different grids at fully developed region about outlet of 3D tube

Fig. 2 shows typical grid independence study conducted for x-velocity profiles for  $Re=100$ . Around 223080 mesh points are the optimal number to obtain grid independent solution.

Fig. 3 exhibits the comparison of mean WSS coefficient between numerical and analytical solution [20]. It can be seen from the figure that the WSS coefficient computed on the coarser grid agrees very well with analytical solution.



**Fig. 3** Comparison of computed mean WSS coefficient at different dimensionless axial locations with the analytical solution [20] at Re=100

Four different mesh testing procedures are conducted to guarantee the grid-independency of the present stenosis models. Mean WSS value for various mesh combinations are explored for the case of Re=340 for Newtonian blood flow as shown in Table 1.

**Table 1** Comparison of the average wall shear stress coefficient for different grid resolution for all stenosis models at Re=340

| Mesh size | S=45%   | S=55%  | S=65%  | S=75%  |
|-----------|---------|--------|--------|--------|
| 20×20×530 | 31.5812 | 31.084 | 30.516 | 36.304 |
| 24×24×580 | 31.612  | 31.109 | 30.541 | 36.339 |
| 27×27×631 | 31.622  | 31.125 | 30.551 | 36.348 |
| 30×30×680 | 31.628  | 31.130 | 30.558 | 36.354 |

#### 4 RESULTS

CFD simulations are carried out on the symmetric stenosis model with different degrees of stenosis 45%, 55%, 65%, and 75% at Reynolds numbers 130, 160, 190, and 340. The governing equations are discretized by using the control volume method in body-fitted coordinates. The SIMPLE algorithm is used to ensure the coupling between velocity and pressure. The convection and diffusion terms are discretized by the power-law and central scheme, respectively. First of all, Fig. 4 demonstrates the geometry of the straight symmetrical stenotic tube and computational grids for the stenosis models with 612,000 volume cells. In order

to improve the quality of the generated grid system, especially at stenosis region, some controlling parameter like Skewness value and MAR are calculated for each cell. Table 2 presents MAR for all cases in this study.

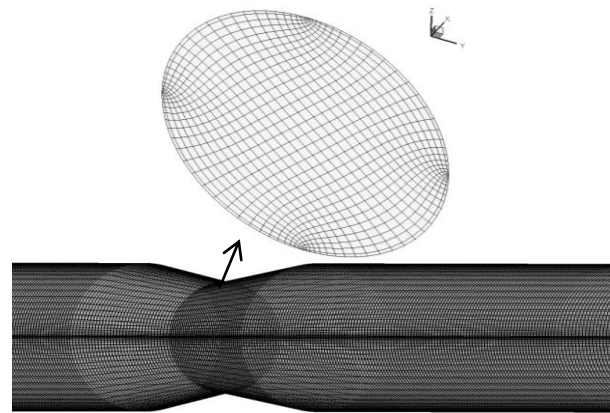


**Fig. 4** 3D elliptic grid at stenosis model

**Table 2** Calculating MAR of computational cells in different models

| simulation models | maximum MAR in domain | mean MAR in domain |
|-------------------|-----------------------|--------------------|
| cylinder          | 25                    | 1                  |
| 45% stenosis      | 25                    | 1                  |
| 55% stenosis      | 25                    | 1                  |
| 65% stenosis      | 25                    | 1                  |
| 75% stenosis      | 25                    | 1                  |

Table 3 presents maximum, minimum, and mean values of Skewness for computational cells in all models. A right-angled cell has the skewness value of one. For a degenerate cell, the skewness Value is zero. As the cells having more right-angled, their skewness value becomes smaller. In this study, all computational models have acceptable grid quality corresponding to the Table 2 and Table 3.

**Table 3** Calculating Skewness of computational cells in different models

| simulation models | maximum Skewness in domain | minimum Skewness in domain | mean Skewness in domain |
|-------------------|----------------------------|----------------------------|-------------------------|
| cylinder          | 0.9966                     | 0.4989                     | 0.9                     |
| 45% stenosis      | 0.9966                     | 0.2393                     | 0.8                     |
| 55% stenosis      | 0.9966                     | 0.2245                     | 0.8                     |
| 65% stenosis      | 0.9966                     | 0.2205                     | 0.8                     |
| 75% stenosis      | 0.9966                     | 0.2045                     | 0.8                     |

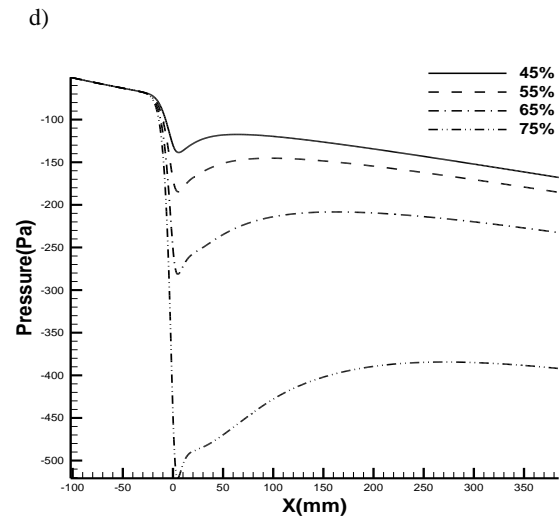
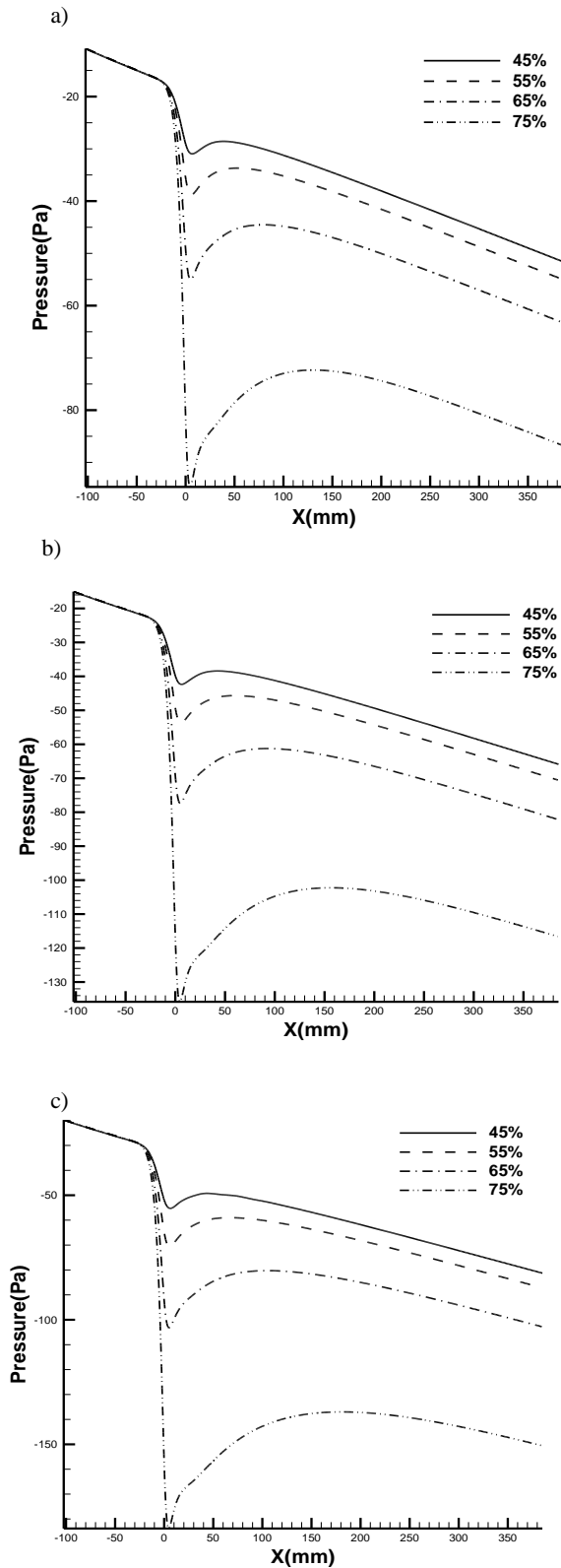


Fig. 5 Comparison of pressure distribution along the models wall for different degrees of stenosis at (a) Re= 130 (b) Re=160 (c) Re=190 and (d) Re=340

Pressure within the artery is an important characteristic as it can determine the resistance against the flow in the vessel. A large pressure drop across the vessel causes the flow experience resistance and has a tendency to stagnate or even reverse (an undesirable feature). Figure 5 shows the pressure distributions along all stenosis models for four different Reynolds number with 130, 160, 190, and 340. A rapid fall in pressure is observed as the occlusion is approached, and the local minimum is attained corresponding to the separation point in all models.

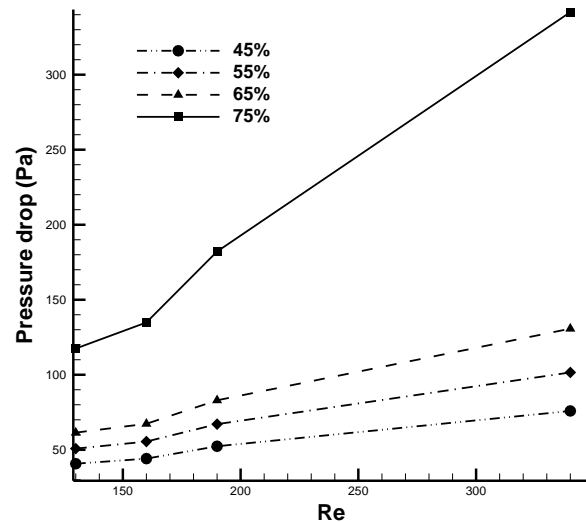


Fig. 6 Comparison of pressure drop along stenosis models with different degrees of stenosis versus Reynolds number

Furthermore, distribution of pressure drop versus Reynolds numbers for different degrees is presented in Fig. 6. It is clear that with increasing degree of stenosis,

the increase in pressure drop through stenosis model increases significantly. In case of 75% stenosis, fast decrease in pressure (Fig. 5 frame d) by passing through constriction, causes highly increase of pressure drop especially at high Reynolds number.

Fig. 7 shows the contour plots of streamlines of the flow through different degrees of stenosis at four different Reynolds numbers. The separated shear layer at the neck of stenosis due to the adverse pressure (existing downstream of stenosis), reattaches to the wall at downstream of stenosis. This reattachment causes to form a vortex in this region at some cases. The corresponding lengths of the major axes are presented in Table 4. It is also noticed that the length of the vortexes are increased with the increasing Reynolds number and degrees of stenosis.

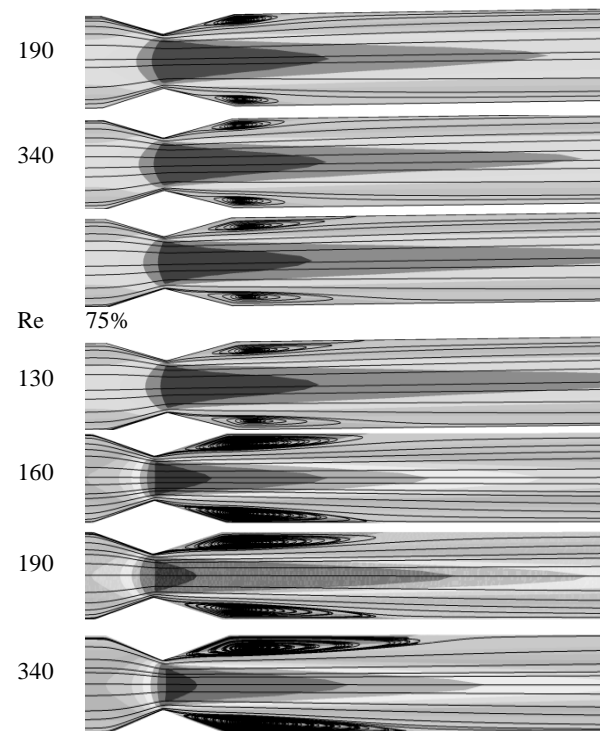
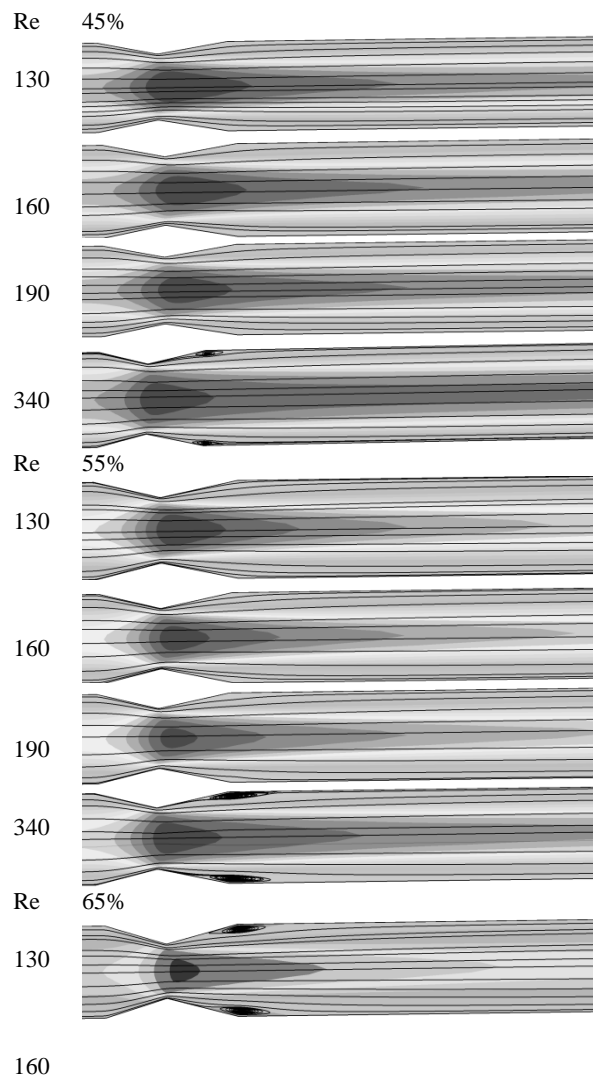
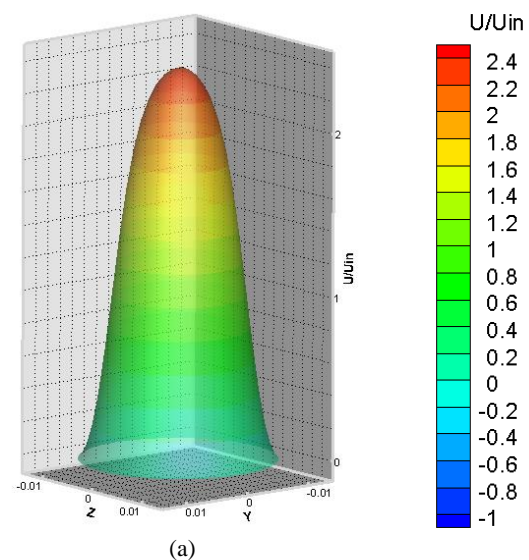
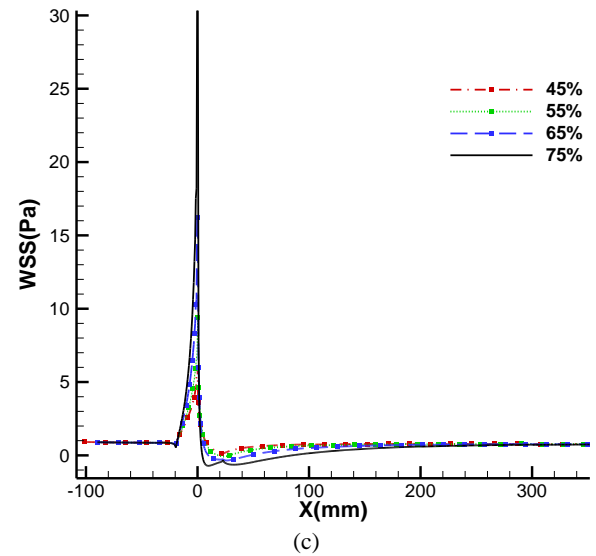
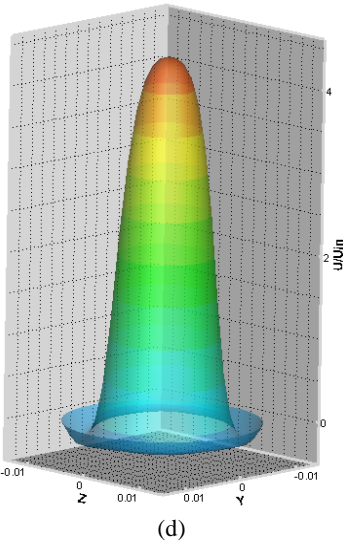
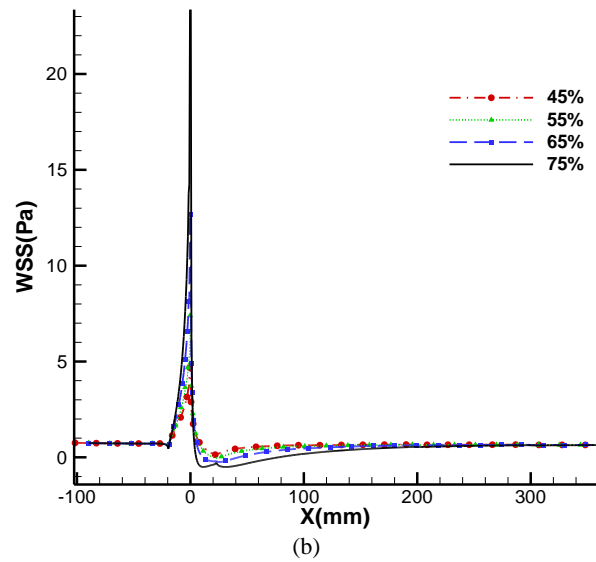
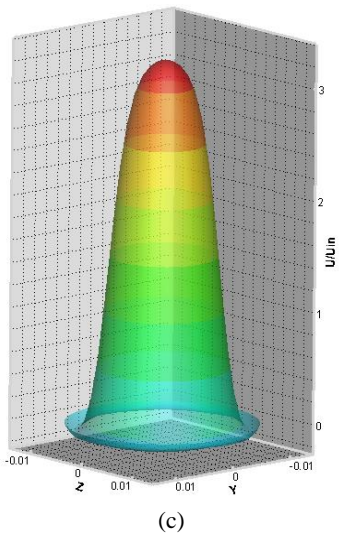
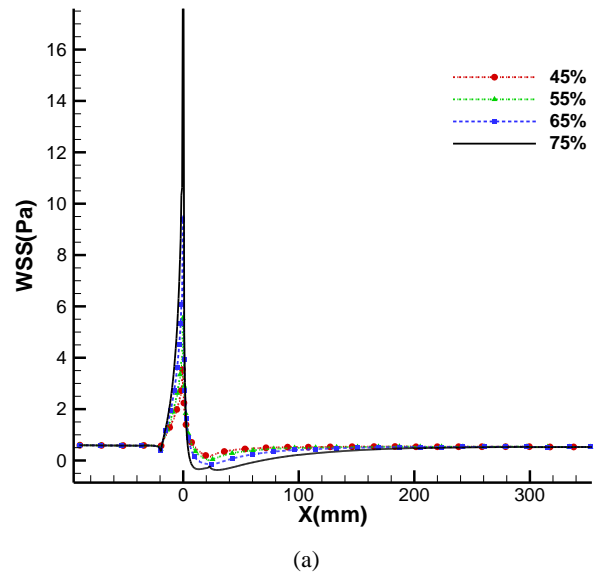
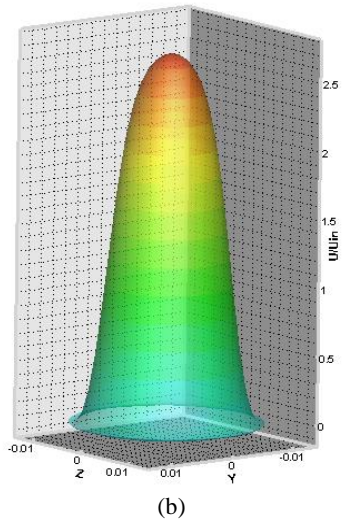


Fig. 7 Contour plots of streamlines at different degrees of stenosis and different Reynolds number

This could be an alarming condition. Because, from pathological point of view, the blood in the post-stenosis region is re-circulated for a long time and stagnant in this region, which could potentially cause the blood clot or thrombosis leading to stroke and heart attack.





**Fig. 8** 3D contour plots of stream wise velocity in the cross-section at downstream of stenosis for different degrees of stenosis a) S=45% b) S=55% c) S=65% d) S=75% at Reynolds number 340

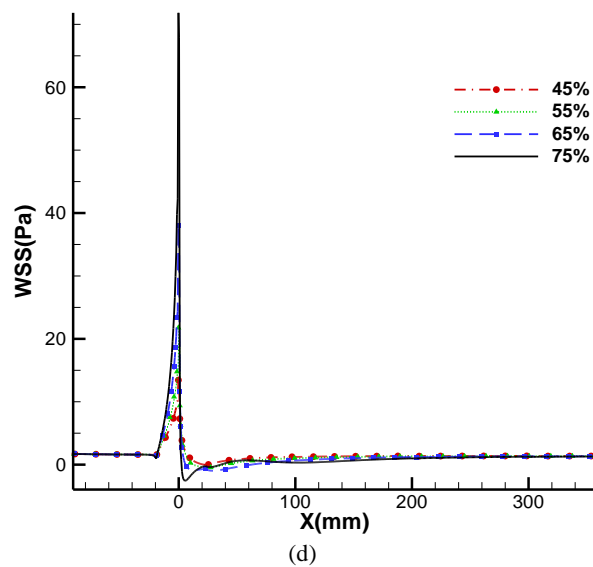


Fig. 9 Comparisons of WSS at different degrees of stenosis for a) Re=130 b) Re=160 c) Re=190 and d) Re=340

Table 4 Length of vortices generated downstream of stenosis with different degrees for Reynolds number 130, 160, 190, and 340 corresponding the contour plot of stream lines at Fig. 7

| Re  | vortex length<br>S=45% | vortex length<br>S=55% | vortex length<br>S=65% | vortex length<br>S=75% |
|-----|------------------------|------------------------|------------------------|------------------------|
| 130 | -                      | -                      | 0.64 D                 | 2.22 D                 |
| 160 | -                      | -                      | 0.81 D                 | 2.3 D                  |
| 190 | -                      | -                      | 0.95D                  | 2.49D                  |
| 340 | 0.44D                  | D                      | 1.62D                  | 3.25D                  |

Figure 8 compares 3D contour plots of stream wise velocity at the cross-section downstream of stenosis for different degrees of stenosis at Reynolds number 340. It is readily apparent that the recirculation regions observed in Fig. 8 are associated with regions of low pressure. Within such recirculation regions indicated by the negative velocity (blue color), blood moves in the direction opposite to the mean flow, increasing the probability of stenosis.

Figure 9 shows comparisons of WSS for 45%, 55%, 65%, and 75% area reductions at different Reynolds number. It is also clear that with increasing degree of stenosis and Reynolds number, magnitude of WSS increases significantly, and this value is the highest at throat of the stenosis. However, a subsequent strong positive-negative oscillation of WSS behind of the stenotic area is found in the case of 65% and 75% area reduction for all Reynolds number and in the case of 45% and 55% area reduction just for Reynolds number 340. These may correspond to the reattachment

locations of the separation zone behind the stenosis on the wall. It is worthwhile pointing out that WSS exceeds the critically reported value ( $40 \text{ n/m}^2$ ) only at 75% stenosis as the velocity reaches its peak value causing damage to the endothelium cell layer.

## 5 CONCLUSION

The numerical simulation of blood flow through an artery with different degrees of stenosis was investigated in this study. Inlet Reynolds numbers of 130, 160, 190, and 340 corresponding to the range of Reynolds number typically involved in the human common iliac artery, which is the most common sites for development of atherosclerotic lesions, were used. An in-house code in Fortran 90 was developed to generate 3D elliptic grids and implement finite volume method in generalized body fitted coordinate in non-rectangular domain. The discretized forms of the transformed equations were obtained by a control volume formulation in a non-staggered grid.

The most important parameters of the simulation were the pressure drop and WSS. It has been hypothesized that the distribution and magnitude of the shear stress and pressure on the arterial walls play a role in the genesis and acceleration of arterial diseases. For instance, local hypertension may be directly caused by localized increase in lateral wall pressure. This study showed that the severity of stenosis had an important effect on the characteristic behaviour of the blood flow. It was found that stenosis model with degree of 75% could be a critical stenosis in this investigation causing the magnitude of WSS exceed corresponding safe bandwidth, where highly pressure drop occurs in this case leading to serious damage to the vessel wall.

Moreover, it was also noticed that the length of the recirculation region and vortices were increased with the increasing Reynolds number and degree of stenosis, which is an alarming condition from pathological point of view. In this case, the blood in the post-stenosis region is re-circulated for a long time and stagnant, which could potentially cause the blood clot or thrombosis leading stroke and heart attack.

## REFERENCES

- [1] Deshpande, M., Giddens, D., "Turbulence measurements in a constricted tube", Journal of Fluid Mechanics, Vol. 97, No. 1, 1980, pp. 65-89.
- [2] Ahmed, S. A., Giddens, D. P., "Velocity measurements in steady flow through axisymmetric stenoses at moderate Reynolds numbers", Journal of Biomechanics, Vol. 16, No. 7, 1983, pp. 505-516.

- [3] Ahmed, S. A., Giddens, D. P., "Pulsatile post-stenotic flow studies with laser Doppler anemometry", *Journal of Biomechanics*, Vol. 17, No. 9, 1984, pp. 695-705.
- [4] Smith, F., "The separating flow through a severely constricted symmetric tube", *Journal of Fluid Mechanics*, Vol. 90, No. 04, 1979, pp. 725-754.
- [5] Deshpande, M., Giddens, D., and Mabon, R., "Steady laminar flow through modelled vascular stenoses", *Journal of Biomechanics*, Vol. 9, No. 4, 1976, pp. 165-174.
- [6] Young, D. F., Tsai, F. Y., "Flow characteristics in models of arterial stenosis-I. Steady flow", *Journal of Biomechanics*, Vol. 6, No. 4, 1973, pp.395-410.
- [7] Mittal, R., Simmons, S., and Najjar, F., "Numerical study of pulsatile flow in a constricted channel", *Journal of Fluid Mechanics*, Vol. 485, 24 June. 2003, pp. 337-378.
- [8] Varghese, S. S., Frankel, S. H., and Fischer, P. F., "Direct numerical simulation of stenotic flows Part 1Steady flow", *Journal of Fluid Mechanics*, Vol. 582, 14 June. 2007a, pp.253-280.
- [9] Varghese, S. S., Frankel, S. H., and Fischer, P. F., "Direct numerical simulation of stenotic flows Part 2 Pulsatile flow", *Journal of Fluid Mechanics*, Vol. 582, 14 June. 2007b, pp. 281-318.
- [10] Sousa, L., Castro, C., Antonio, C., and Chaves, R., "Computational Techniques and Validation of Blood Flow Simulation", *WEAS Transactions on biology and biomedicine, ISI/SCI Web of Science and Web of Knowledge*, Vol. 8, No. 04, 2011, pp. 145-155.
- [11] Singh, S., Shah, R. R., "A numerical model for the effect of stenosis shape on blood flow through an artery using power-law fluid", *Advances in Applied Science Research*, Vol. 1, No. 1, 2010, pp. 66-73.
- [12] Senol, P., Serdar, C., "Analysis of the effects of different pulsatile inlet profiles on the hemodynamical properties of blood flow in patient specific carotid artery with stenosis", *Computers in Biology and Medicine*, Vol. 43, No. 05, 2013, pp. 717-728.
- [13] Golpayeghani, A. T., Najarian, S., and Movahedi, M., "Numerical simulation of pulsatile flow with newtonian and non-newtonian behaviour in arterial stenosis", *Iranian Cardiovascular Research Journal*, Vol. 1, No. 03, 2008, pp. 167-174.
- [14] Kaul, U. K., "Three-dimensional elliptic grid generation with fully automatic boundary constraints," *Journal of Computational Physics*, Vol. 229, No. 17, 2010, pp. 5966-5979.
- [15] Farrashkhalvat, M., Miles, J., "Basic Structured Grid Generation: With an introduction to unstructured grid generation", *Butterworth-Heinemann, Britain*, 2003, Chaps. 4, 5.
- [16] Akcelik, V., Jaramaz, B., and Ghattas, O., "Nearly Orthogonal Two-Dimensional Grid Generation with Aspect Ratio Control", *Journal of Computational Physics*, Vol. 171, No. 2, 2001, pp. 805-821.
- [17] Lehtimäki, R., "An algebraic boundary orthogonalization procedure for structured grids", *International journal for numerical methods in fluids*, Vol. 32, No. 5, 2000, pp. 605-618.
- [18] Fletcher, C. A. J., "Computational Techniques for Fluid Dynamics 2", *Springer*, 1991.
- [19] Pedley, T. J., "The fluid mechanics of large blood vessels", *Cambridge University Press, Cambridge*, 1980.
- [20] Bejan, A., "Convection heat transfer", *John Wiley & Sons, Canada*, 2004.